Preparation and characterisation of biochars from elephant grass and their utilisation for aqueous nitrate removal: Effect of pyrolysis temperature

Article *in* Journal of Environmental Chemical Engineering · December 2020

DOI: 10.1016/j.jece.2020.104507

CITATIONS
0

READS
43

6 authors, including:

Matthew Adebayo
The Federal University of Technology, Akure, Ondo State, Nigeria.
51 PUBLICATIONS **1,056** CITATIONS
SEE PROFILE

Emmanuel Olasehinde
Federal University of Technology, Akure
28 PUBLICATIONS **189** CITATIONS
SEE PROFILE

Labunmi Lajide
Federal University of Technology, Akure
77 PUBLICATIONS **246** CITATIONS
SEE PROFILE

Journal of Environmental Chemical Engineering 8 (2020) 104507

Contents lists available at ScienceDirect

Journal of Environmental Chemical Engineering

journal homepage: www.elsevier.com/locate/jece

Preparation and characterisation of biochars from elephant grass and their utilisation for aqueous nitrate removal: Effect of pyrolysis temperature

Mibinuola Florence Adesemuyi [a], Matthew Ayorinde Adebayo [a,*], Adebisi Olayinka Akinola [b], Emmanuel Folorunso Olasehinde [a], Kehinde Abiodun Adewole [b], Labunmi Lajide [a]

[a] Department of Chemistry, The Federal University of Technology, Akure, Nigeria
[b] Department of Mechanical Engineering, The Federal University of Technology, Akure, Nigeria

ARTICLE INFO

Editor: Despo Kassinos

Keywords:
Elephant grass
Biochar
Nitrate ion
Pyrolysis
Liu isotherm
Avrami fractional order

ABSTRACT

Biochar is a solid material obtainable from biomass pyrolysis and useful for pollution alleviation and soil amendment. In this study, Biochars A and B were produced from elephant grass at pyrolytic temperatures of 400 °C and 600 °C, respectively, for removal of nitrate ion from aqueous solution. The physicochemical characteristics of the biochars were evaluated. The biochars were also characterised using Fourier Transform Infrared (FTIR) spectroscopy, Scanning Electron Microscopy (SEM), Energy Dispersive X-ray (EDX), and X-ray Diffraction (XRD). Operational variables such as pH, contact time, and concentration of nitrate ion were varied and optimum variables were obtained. Kinetic and equilibrium data were subjected to kinetic (pseudo-first order, pseudo-second order, Avrami fractional order, Elovich and intraparticle diffusion) and equilibrium (Langmuir, Freundlich, Liu, and Redlich-Peterson) models, respectively, to elucidate the interaction between the nitrate ion and biochars. The yields of Biochars A and B were 41.40 % and 32.25 %, respectively. The two biochars possessed good cation exchange capacity, water-holding capacity, carbon stability, and porosity. Avrami fractional kinetic order was the best model that explained the kinetic data. Maximum adsorption capacities obtained from Liu model (the best equilibrium model) are 140.7 and 237.5 mg g^{-1} for Biochars A and B, respectively. Adsorption process was spontaneous and exothermic. There was a decrease in the disorderliness in the nitrate-biochar system. Biochar B performed better than Biochar A for removal of nitrate ion from water. In summary, the biochars produced from elephant grass excellently removed nitrate ion from solution and could be utilised for water decontamination.

1. Introduction

Agricultural wastes (biomass) are being turned out in large quantities yearly by many countries as the population growth increases. It is disheartening to know that some of the agricultural wastes are thrown away without utilising them for constructive purposes. Indiscriminate disposal of biomass eventually results in environmental pollution and various health challenges for living organisms including man [1,2]. Unwanted and dangerous gases are released enormously into the atmosphere when agricultural wastes decompose and fossil fuel is burned. Agricultural sector is a major source of atmospheric greenhouse gases (GHGs) and, in most cases, the majority of the emitted GHGs are not consumed. Emission of CO_2 (one of the GHGs) as a result of soil respiration is quite higher than the emission from burning of fossil fuels [3]. Tilling of agricultural fields, burning of fossil fuels, and excessive deforestation bring about movement of carbon from the lithosphere and biosphere to the atmosphere higher than the amount plants can utilise for photosynthesis [3]. A number of problems in our planet earth are due to an increase in the atmospheric concentration of GHGs being released into the atmosphere [4]. Therefore, it is important to reduce the emission of GHGs from agricultural soil so as to alleviate the challenges of climate change. Environmental pollution undoubtedly constitutes a great danger to the ecosystem. In view of the problems emanating from careless disposal of the biomass in the ecosystem, there is an urgent call for optimal biomass utilisation for reduction in diverse environmental issues ranging from GHGs emission to pollution, leaching of soil nutrients and pandemic [5,6]. The good news is that there are reduction technologies, such as energy conservation and the usage of renewable energy, for emission of GHGs. The presence of biochar in soil can indirectly reduce the emission of GHGs [3].

* Corresponding author.
E-mail address: adebayoma@futa.edu.ng (M.A. Adebayo).

https://doi.org/10.1016/j.jece.2020.104507
Received 4 August 2020; Received in revised form 4 September 2020; Accepted 15 September 2020
Available online 22 September 2020

Nitrogen exists in soil in form of organic nitrogen compounds, nitrate and ammonium, however, nitrate is the main form of nitrogen that plants consume. Nitrate contamination in the soil arises from application of nitrogen fertilisers (such as ammonium sulphate), livestock manure, aquaculture baits, sewage and septic wastes [7]. Nitrate is one of the most widespread pollutants in drinking water [8] because nitrate run-off is a source of eutrophication (nutrient accumulation in soil), which is accelerated *via* anthropogenic activities. Eutrophication process degrades the water ecosystem and could lead to fish death, algal bloom, and economic loss [9]. Nitrate is a groundwater pollutant and its presence in potable water constitutes a risk to human health and can cause methaemoglobinemia (blue baby syndrome) and cancer in children [10]. High concentration of this pollutant in agricultural soil can equally result in several environmental damages. The challenges pose by the presence of nitrate in water have made World Health Organization (WHO) to set threshold limit of < 50 mg/L as the permissible concentration of nitrate-nitrogen in drinking water [11].

Conventional water treatment techniques, such as filtration and lime softening, cannot be used for elimination of nitrate ion from water because nitrate is highly soluble and stable in water [12]. There are many viable methods for nitrate removal in water. Some of the nitrate removal methods are biological denitrification, electrodialysis, reverse osmosis, ion exchange and adsorption [10]. There are many limitations to the usage of some of the aforementioned methods. Some of the methods are slow and inefficient while installation and maintenance cost of some of these methods is high [13]. Specifically, ion exchange resins have selectivity problem and the resins may retain other anions that can destabilise equilibrium of the ionic composition [14] while biological denitrification requires specific microorganisms for performance [12]. Adsorption method is the most outstanding, simplest, best, most efficient and most economical method for nitrate ion uptake from water [15,16].

Biochar is a stable carbon-rich solid product obtained when biomass is thermally decomposed (pyrolysed) in a closed system or in a system of restricted air conditions between 350 °C and 700 °C [17]. Pyrolysis thermally decomposes the carbohydrate structure of biomass into carbonaceous solid residue (biochar), and condensable and non-condensable vapours of diverse compounds of different molecular weights. Biochar is a value-added product that can be used for various purposes such as energy production, soil remediation and fertilisation, reduction of greenhouse gas emission, carbon sequestration, and adsorption of pollutants [18–21]. When biochar is added to soil, it buffers the pH, increases the water-holding capacity and increases the cation exchange capacity of soil. Biochars are also good materials for retention of hazardous compounds [15].

Elephant grass is a perennial native weed of Africa, which is used as forage for livestock. The scientific name of elephant grass is *Pennisetum purpureum* Schum. It is a tufted grass that can grow up to 4 m high with pale green leaves (up to 4 cm width). It has a strong midrib tapering to a fine point and the grass can be used for ornamental purposes and structural landscaping [22]. Elephant grass is a widely cultivated plant and can spread by man, wind and water. In appearance, the grass is similar to sugar cane but has narrower leaves and shorter than sugar cane that can grow up to 6 m [23].

Agricultural wastes can be used in their native form for removal of nitrate ion from water, however, their usage is marred with low adsorption capacities in most cases [12]. The agricultural wastes can therefore be converted to biochars for improvement in adsorption features. Biochars have been prepared from a number of different kinds of biomass, such as corncob [16], Douglas fir [24], sugarcane bagasse and wood chips [25], sawdust [26], oak sawdust [27], birch wood [28], wheat straw [29], soybean [30], and used for removal of nitrate ion from aqueous solutions. The chemical and physical characteristics of biochars depend on various factors such as the nature of the biomass feedstock, residence time, reaction rate, and temperature of the pyrolysis [25,31,32]. The temperature of pyrolysis of biochars has tremendous impact on the characteristics of biochars and this greatly influence the ability of biochars to adsorb pollutants from aqueous solutions [33]. Zhao et al. [16] prepared three types of biochars from corncob at three pyrolytic temperature values (300 °C, 450 °C, and 600 °C). The biochars were used for nitrate ion removal from aqueous solutions and it was found that the biochar produced at 600 °C was the best adsorbent for nitrate removal. In another study reported by Kameyama et al. [25], the of biochars pyrolysed at 800 °C gave the best adsorption of NO_3-N than those pyrolysed at 400 °C and 600 °C. Similarly, date palm biochar produced at 700 °C exhibited higher efficiency for removal of NO_3–-N from aqueous solutions than the one pyrolysed at 300 °C [31]. This observation was also supported by the report of Zhou et al. [26]

There is an emergent demand for development of effective technologies for removal of nitrate from natural water system. The idea of this research was conceived to evaluate the possibility of using elephant grass as feedstock for production of biochars and to probe further the effect temperature on biochar characteristics. Other specific objectives are to: (1) evaluate the adsorption properties of the elephant grass biochars for removal of nitrate ion (NO_3^-) from aqueous solutions, (2) assess the adsorption characters of biochars by varying the pH, contact time and concentration of nitrate ion in solution, and (3) evaluate the adsorption data using kinetic models (pseudo-first order, pseudo-second order, Avrami fractional order, Elovich and Intraparticle diffusion), equilibrium models (Langmuir, Freundlich, Liu, and Redlich-Peterson) and thermodynamic equations such as van't Hoff equation.

2. Materials and methods

2.1. Preparation of biochars

All the reagents used in this work were of analytical grades and used without further treatment. The solutions were prepared using double distilled water. The biomass, elephant grass (*Pennisetum purpureum* S.), was collected from the Teaching and Research Farm of The Federal University of Technology, Akure, Nigeria. The biomass, which was used as feedstock or precursor for the research work, was washed, cut into small pieces, sun-dried for 21 days, subsequently oven-dried for 24 h at 105 °C in the laboratory, and stored in a clean polythene bag until usage.

Biochars were produced from the dried elephant grass using a locally constructed fixed-bed slow pyrolytic reactor (thermochemical reactor) of *ca.* 17.4 L capacity. The reactor consisted of pyrolytic canister, furnace, condensing unit, digital electronic control unit, water reservoir, water pump flow meter, control valve, and interconnected pipe for collection of liquid and gas products. The reactor can withstand pressure of 2.3 MN/m^2 and temperature up to 1200 °C [34]. The temperature of the reactor was set at 400 °C and 600 °C to produce Biochars A and B, respectively. The biochar was the residual product inside the reactor after pyrolysis. The two biochars produced in this study were not chemically modified because they were also used for soil amendment [35].

2.1.1. Characterisation of Elephant grass and biochars

The percentage yield, elemental composition, ultimate, and physicochemical analyses of the elephant grass and biochars were investigated using standard methods, such as Official Methods of Analysis of the Association of Official Analytical Chemists (AOAC) and American Society for Testing Materials–Miscellaneous Materials (ASTM D-2866) methods. The elephant grass and the Biochars A and B were also characterised using Fourier Transform Infrared (FTIR) spectroscopy, Scanning Electron Microscopy (SEM), Energy Dispersive X-ray (EDX), and X-ray Diffraction (XRD) spectroscopy.

The yield in percentage of biochar was determined from the mass of the biochar obtained after pyrolysis and the mass of dried elephant grass used for pyrolysis as shown in Eq. (1).

$$Yieldofbiochar(\%) = \frac{massofbiochar(g)}{massofelephantgrass(g)} \times 100 \quad (1)$$

The percentage yield of liquid condensates was evaluated using Eq. (2). The percentage of non-condensable gaseous products was determined using Eq. (3).

$$Yieldofliquidcondensate(\%) = \frac{massofliquid(g)}{massofelephantgrass(g)} \times 100 \quad (2)$$

$$\%ofgaseousproduct = 100 - (\%yieldofbiochar + \%yieldofliquidcondensate) \quad (3)$$

The elemental (CHN) analysis was performed using Elemental Analyser (Thermo Fisher Scientific 2000) while the amounts of extractable macro- and micro-nutrients (N, P, K, Na, Ca and Mg) were determined using Inductively-coupled Plasma-Mass Spectroscopy (PerkinElmer) after acid digestion of the biochars.

Fourier transform infrared spectroscopy is an efficient characterisation tool for identification of functional groups present in an unknown sample [36]. The powdered samples and KBr were separately oven-dried at 105 °C for 6 h, and stored in a desiccator for 72 h before FTIR analysis. The FTIR of the samples were recorded over a scanning range of 500 cm^{-1} to 4000 cm^{-1} on FTIR spectrophotometer (Perkin Elmer, PE 100). The elephant grass and the biochars were prepared for SEM/EDX by double coating the samples with palladium in order to charge the samples. The micrographs were measured at an accelerating voltage of 15 kV on JEOL JSM-639OLV scanning electron microscope to determine the surface morphologies of the samples. The EDX analysis was carried out to determine the elemental composition of the samples. Samples were carbon sputtered and the corresponding cross-sections were analysed at accelerating voltage of 15 kV. The quantification of the potassium/carbon intensity ratio was added up to 100 % at the surface for each sample. X-ray diffractograms of the samples were obtained using Shimadzu diffractometer (XRD-600) with monochromatic Cu Kα radiation (λ =0.1542 nm).

2.2. Preparation of solutions and procedure for adsorption study

A 1.0 g/L of the stock nitrate solution was prepared by weighing an accurate mass of potassium nitrate (KNO_3) and dissolving it using double distilled water. Different working solutions of nitrate ion were prepared from the stock solution by serial dilution using double distilled water.

Adsorption experiments were performed three times using batch adsorption methods to test the potentials of Biochars A and B, prepared from Elephant grass, as adsorbents for removal of nitrate ion (NO_3^-) from the aqueous solutions. For a routine adsorption procedure, 50.0 mg of adsorbent was put into different 25 mL round bottom Falcon tubes, each containing 20.0 mL of nitrate solution (10–200 mg/L), which was shaken thermostatically for a period (0–480 min) to achieve equilibrium at a constant agitation speed of 160 rpm and at temperature ranging from 298 K to 323 K. The initial pH values of the nitrate solutions ranged from 6.4 to 6.8. The pH of each solution was adjusted to a desired value (2.0–10.0) by drop-wise addition of 0.1 mol/L HCl or 0.1 mol/L NaOH. The optimum pH was determined as the pH with the highest adsorption of nitrate ion. It was on this premise that all other studies were investigated. After adsorption experiment, nitrate-adsorbent system was centrifuged to separate the spent adsorbent. To calculate the concentration of nitrate ion remaining in the solution, the absorbance of the nitrate solution was measured at wavelengths of 220 nm and 275 nm [7,10,30] using a double beam UV–vis spectrophotometer (Shimadzu Model 1800). When necessary, an aliquot of the clear supernatant was properly diluted with distilled water of specific pH before taking absorbance readings. The percentage removal of nitrate ion and amount of nitrate ion removed (by the Biochars A and B) were calculated by applying Eqs. (4 and 5), respectively.

$$AdsorptionEfficiency = \frac{(C_o - C_e)\cdot 100}{C_o} \quad (4)$$

$$q_e = \frac{(C_o - C_e)\cdot V}{m} \quad (5)$$

In the above equations, q_e is the amount of nitrate ion adsorbed by the biochars in mg/g, C_o is the initial nitrate ion concentration that was in contact with the biochars in mg/L, C_e is the nitrate concentration after the batch adsorption procedure in mg/L, m is adsorbent mass in g, and V is the volume of nitrate solution in L.

2.3. Statistical analysis and data modelling

The data obtained were subjected to statistical analysis to test the significance differences, which were done using ANOVA (one-way analysis of variance) and Duncan's new multiple range test (DMRT) with a $p < 0.05$ that indicated significance. Statistical package for Social Science (SPSS) version 20 was used for these tests.

Adsorption data were obtained in three replicates and the means of experimental data were used. The kinetic and equilibrium adsorption data were fitted to non-linear models using OriginPro 9.6. The kinetic models used were pseudo-first order, pseudo-second order, Avrami fractional order, Elovich and intraparticle diffusion while Langmuir, Freundlich, Liu, and Redlich-Peterson were the equilibrium models used in this study. The values of adjusted determination coefficient (R^2_{adj}) and standard deviation (SD) were used to determine the model of the best fit.

3. Results and discussion

3.1. Physicochemical characteristics of the elephant grass and biochars

At the end of the slow pyrolysis of elephant grass, three different products namely; biochar (solid), liquid condensates (bio-oil and bio-tar) and non-condensable gases were obtained [35,37,38]. Pyrolysis temperatures of 400 °C and 600 °C were used to obtain Biochars A and B, respectively. The percentages of biochar, liquid condensates and gases are *ca.* 41 %, 43 % and 16 %, respectively, for Biochar A. The respective percentages are about 32 %, 58 % and 10 % for Biochar B. Table S1 presents the physicochemical data of the elephant grass and the two biochars produced. The yields of the biochars decreased from 41.40 % to 32.25 % as the temperature was increased from 400 °C to 600 °C. This observation followed results that have been reported earlier [39,40]. High pyrolysis temperature is associated with an increase in the amount of water and volatile compounds as biomass decomposed [40]. As shown in Table S1, the percentage of moisture content of dried elephant grass was 10.20 %. This value decreased to 4.80 % (Biochar A) and 2.73 (Biochar B). The moisture content of feedstock has a significant effect on the thermal process, because it affects heating value directly [41]. For pyrolysis, an extra heat is required for vaporising the moisture content of feedstock that contains high water content. Similarly, the reduction in biochar yield with an increase in temperature may be related to transformation of lignocellulosic composition of the biomass and also, to dehydration of hydroxyl group [42]. Biochar production is always favoured at lower pyrolysis temperature because condensation of aliphatic compound at lower pyrolysis temperature is minimal.

The pH of elephant grass was determined as 9.33, this value increased to 10.36 and 10.82 for Biochars A and B, respectively. The elephant grass biomass and the biochars were alkaline; the results agreed with earlier reports [43,44]. The elephant grass is rich in fibre (41.97 %), cellulose (37.67 %) and hemicellulose (21.15 %). Significant increase in ash content of elephant grass from 4.93 % (raw) to 23.91 (Biochar A) and 30.00 (Biochar B) was expected because more organic components of biomass were pyrolysed at higher temperature.

The percentage of volatile matter of elephant grass was 82.44 %, which is higher than the values reported in literature. The variation may

be due to plant chemical compositions and some environmental factors. Although, volatile matter composition insignificantly affects the release of stronger bonds during thermal conversion of biomass, however, the performance of feedstocks and the stability of the thermal conversion products are significantly affected. High quantity of volatile matter of the elephant grass biomass is associated to fast ignition potential of the pyrolysis [41]. The values of organic, carbon, ash content, exchangeable acidity, cation exchange capacity, and electrical conductivity are directly proportional to temperature of pyrolysis while the values of carbon stability, water-holding capacity and unstable organic carbon are inversely proportional to pyrolytic temperature. Other properties of the elephant grass and the biochars are available in Table S1.

The carbon content of feed stocks is important for recognition of their potentials as carbon base application. The biomass used in this research has significant amount of carbon material of 55.67 %. The organic carbon of the biochar increased as the pyrolysis temperature was varied from 400 °C to 600 °C because of the stability of biochar against the biological degradation in soil [42]. Similar results on carbon contents were also reported for different carbonisation temperature values [45]. Comparing these results with earlier studies, it could be said that pyrolysis at elevated temperature promoted the degree of carbonisation of biochars.

Table 1 shows the results of the elemental composition (macro- and micro-nutrients) of the biochars at different pyrolytic temperature values and it is observed from the table that nitrogen value of the biochar increased as the pyrolysis temperature increased from 400 °C to 600 °C, the nitrogen values increased from 0.20 to 0.31 %. Therefore, the biomass feed stocks are environmentally friendly energy sources since they all contain trace amounts of nitrogen. However, it could be deduced from Table 1 that the nutrients in Biochar A are higher than those in Biochar B.

3.2. Ultimate analysis of the elephant grass and the biochars

The results of ultimate analysis gave the chemical composition of the elephant grass and the biochars as shown in Table 2. The reported data showed that carbon content of the native biochar increased from 34.24 % (elephant grass) to 77.76 % (Biochar B). High pyrolysis temperature resulted in production of biochar with high carbon content; at the same time, elevated temperature aided the loss of hydrogen as a result of cleavage of weak bonds in biochar [46]. The percentages of O, H and S contents decreased significantly as pyrolytic temperature was increased from 400 °C (Biochar A) to 600 °C (Biochar B). The percentages of O (58.87 %) and H (5.20 %) present in elephant grass are comparable with the values that have been reported earlier [47,48]. The results showed that the percentages of N-contents are almost the same for the elephant grass and biochars. Alsewaileha et al. [31] observed a decrease in N-content of biochar when temperature was increased from 300 °C to 700 °C. Kameyama et al. [25] reported characteristics of seven different biochars but the percentages of the N-contents of the biochars did not follow a regular pattern. Hence, the percentage of N-content of biochar may not depend on the pyrolytic temperature. The calculated atomic ratios of O/C; H/C and (O + N)/C decreased gradually with increased in pyrolytic temperature. The gradual reduction of H/C in the biochar is an indication of effective carbonisation of the biomass while a decrease in the ratio of O/C is attributed to polarity reduction and the hydrophilicity

Table 2
Ultimate analysis (CHOSN) of elephant grass and biochars.

	C	N	H	O	S	H/C	O/C	(O + N)/C
Elephant grass	34.24	1.49	5.20	58.87	0.20	0.15	1.72	1.76
Biochar A	45.95	1.51	3.32	49.06	0.16	0.07	1.07	1.10
Biochar B	77.76	1.57	1.86	17.90	0.05	0.02	0.23	0.25

nature of the biochar surface [49]. The ratio of H/C and O/C were used as an indicator for carbonisation and reduction in this ratio showed that there was a loss of water and O-containing functional groups at high pyrolytic temperature, which decreased the alkyl carbon content but increased the formation of aromatic carbon [50].

3.3. Fourier transform infrared analysis of the biomass and biochars

Fig. 1 shows the Fourier transform infrared spectra for elephant grass and biochars. The spectra show that the biochars and the biomass contained mainly the following functional groups: hydroxyl group, carbonyl group, carboxyl group, ether group, and aromatic C═N [51,52]. The bands of FTIR spectra of the biochars and the elephant grass were

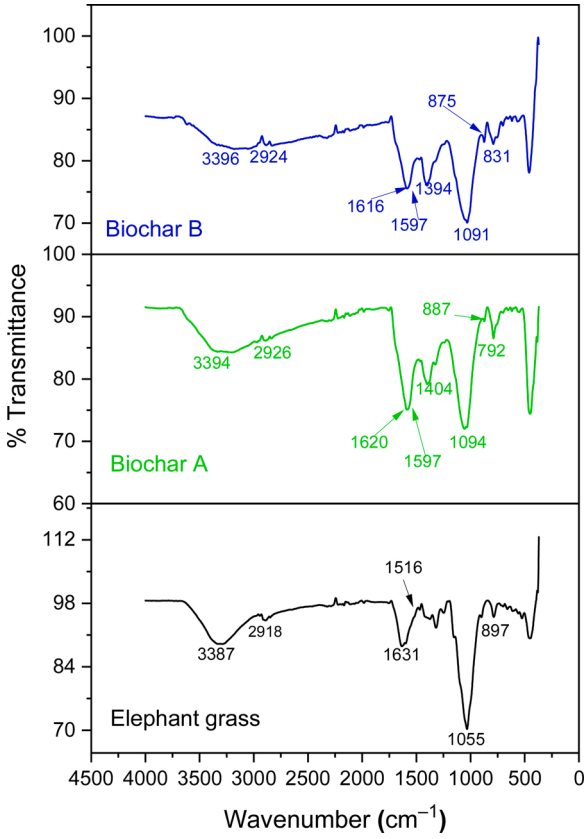

Fig. 1. FTIR spectra of elephant grass, Biochar A and Biochar B.

Table 1
Elemental compositions of elephant grass biochars.

Biochar	(mg/100 g)			(C mol/kg)		
	N	P	K	Na	Ca	Mg
Biochar A	0.20^{b}±0.01	35.34^{b}±1.00	2.59^{b}±0.01	1.82^{b}±0.01	3.35^{a}±0.05	1.40^{a}±0.01
Biochar B	0.31^{a}±0.01	32.14^{b}±0.01	2.19^{b}±0.01	1.67^{b}±0.01	2.50^{b}±0.10	1.20^{a}±0.10

Values are means of three replicates ± standard deviation. Means in the same column followed by same superscript letter(s) are not significantly different from each other at $p \leq 0.05$.

observed at different peaks: the peaks at 3387 cm^{-1}, 3394 cm^{-1} and 3396 cm^{-1} (for respective elephant grass, Biochars A and B) correspond to OH— stretching, which indicates the presence of phenols and alcohol. The stretching of OH— diminished gradually as the pyrolytic temperature was increased as shown in Fig. 1. This was expected as a result of dehydration of cellulose and hemicellulose components, gas evolution and higher mass loss during thermal decomposition [53,54]. The peaks at 2918 cm^{-1}, 2926 cm^{-1} and 2924 cm^{-1} (Elephant grass, Biochars A and B) correspond to aliphatic CH— stretching vibration. However, CH_2 group was identified in the entire spectra as CH_2 peaks range between 2915 cm^{-1} and 2935 cm^{-1}.

The FTIR data of the elephant grass and biochars reveal that the absorbance of the stretching vibration peaks of CC≡ group (2190 cm^{-1} – 2330 cm^{-1}) increased as the temperature increased and this resulted in an increase in carbonaceous chars. This observation is possibly because of dehydrogenation [55]. The pronounced peaks around 1631 cm^{-1}, 1620 cm^{-1}, 1616 cm^{-1} for elephant grass, Biochars A and B, respectively, could be attributed to the C═C stretching aromatic ring. Besides, there was another evidence for aromatic carbon with the appearance of peaks between 887 cm^{-1} and 875 cm^{-1}. The result is similar to the report of Keiluweit et al. [56]. In addition, the intensities of vibration bands of CC— stretching at 1516 cm^{-1}, 1597 cm^{-1}, 1597 cm^{-1} for elephant grass, Biochars A and B, respectively, are ascribed to the aromatic ring. The peak assignments in the spectra represented aliphatic C—OC— and alcohol −OH (1114 cm^{-1} – 1008 cm^{-1}) [57].

Thermal destruction of cellulose and lignin in the elephant grass resulted in the exposure of aliphatic alkyl CH_2, hydroxyl —OH, ester C═O and aromatic C═O functional groups in biochars [58]. The changes in the peaks and the intensities of all the samples are similar. This shows a strong dependence result of the extent of carbonisation on production temperature [59].

3.4. Scanning electron microscopy (SEM) and energy-dispersive X-ray (EDX) analyses

Scanning electron microscopy (SEM) coupled with energy-dispersive X-ray (EDX) device operating at 15 kV was used to determine the morphologies of the biomass and biochars. For accuracy in data analysis, each EDX analysis was repeated three times and all the results were averaged. The SEM micrographs are presented in Fig. 2. The morphology of the elephant grass (Fig. 2A) revealed that the biomass is fibrous and has a rough surface with rocky and rod-like shape.

The micrographs of the Biochar A (Fig. 2B) and Biochar B (Fig. 2C) show that their surfaces have evenly distributed small pores as a result of destructive volatilisation of organic compounds of lignocellulosic, which resulted in loss of some compounds. The Biochar A displayed bigger pores than Biochar B. This report agreed with that of Shaaban et al. [60] who reported smaller pore sizes for rice husk biochar obtained at 700 °C than those obtained at 300 °C. As the pyrolytic temperature increased, the biochar structure became more uniformed as the number

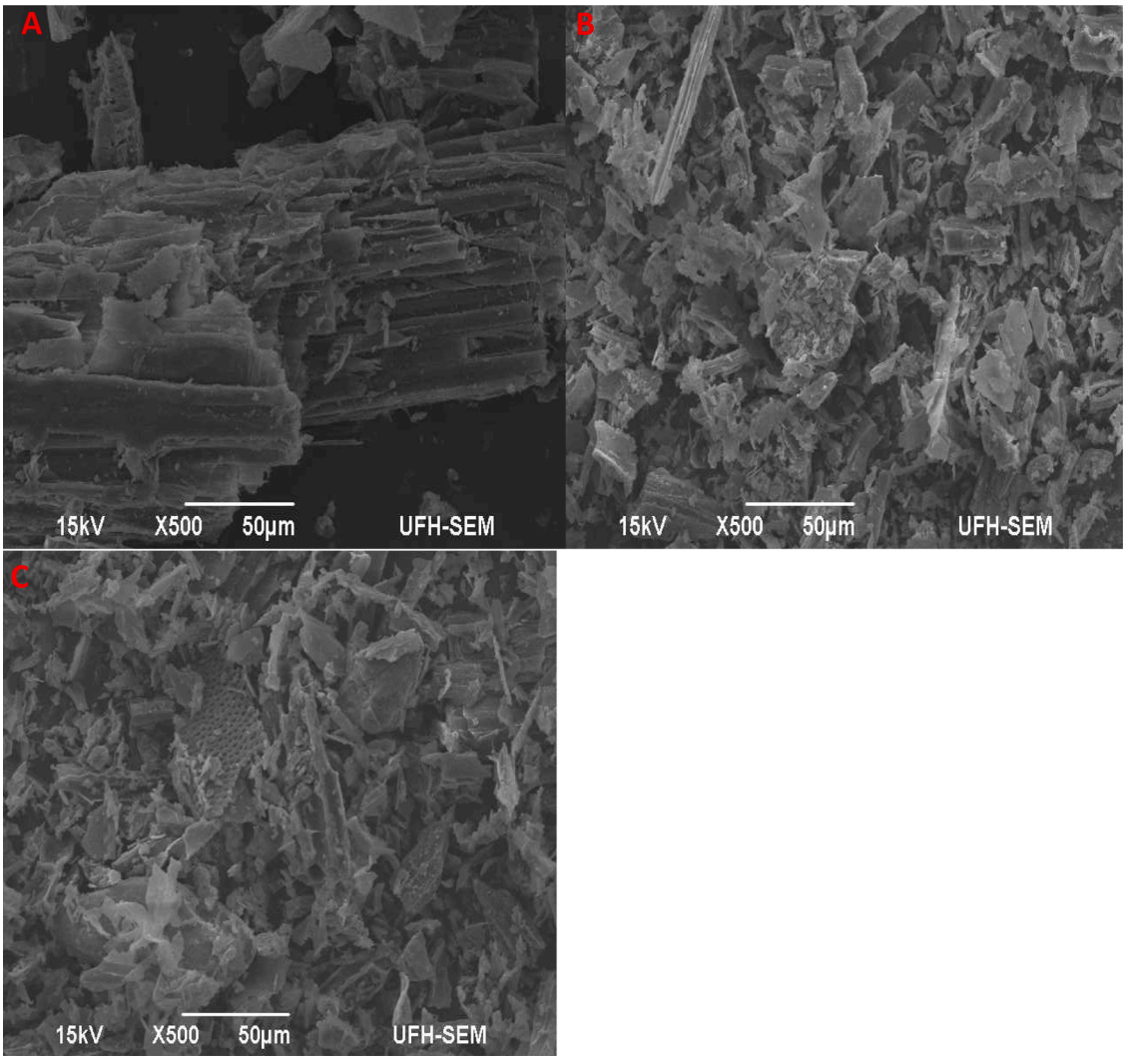

Fig. 2. Scanning electron micrographs of elephant grass (A), Biochar A (B) and Biochar B (C).

of macropores increased and the number of micropores decreased [52]. Apart from good adsorption potentials, the porosities on the surfaces of biochars will also make them relevant in soil amendment because the pores will serve as habitat for microorganisms in the soil. Similarly, porosity will facilitate plant root movement through the soil [60,61].

The average percentages of the EDX elemental mean compositions of elephant grass and biochars are presented in Table 3. The EDX spectra are shown in Fig. S1. Approximately five major elements were identified in the EDX data of biomass and biochars. Carbon, oxygen, potassium, calcium, and silicon are the most abundant elements in the samples. It is visible from the Table 3 that carbon and potassium contents increased significantly as the pyrolytic temperature was increased but the percentage content of oxygen decreased as the charring temperature increased, this phenomenon may be as a result of evaporation of volatile compounds. In addition, the carbon density produced at high pyrolytic temperature is higher than the one obtained at low pyrolytic temperature, which agreed with the results of ultimate analysis.

3.5. X-ray diffraction (XRD) spectroscopy

X-ray diffraction pattern was used to study the crystallinity and amorphousness of both the raw lignocellulosic waste (elephant grass) and the biochars obtained at different temperature values. The results of the XRD are shown in Fig. 3. The intensity of the diffraction patterns was expressed in terms of Bragg's angle (2θ). Two width peaks were detected at 2θ value between 20° and 25°, these regions indicate element with amorphous structure. Both the biochars and the biomass were mostly amorphous in nature but they possessed a few crystalline structures [62]. The amorphous of a biomass structure is determined by the hemicellulose and lignin [60].

The crystallinity structures of the Biochars A and B are displayed distinctively as the pyrolytic temperature was increased because higher temperature increased the volatilisations of organic compounds, which open up more pores, and the XRD patterns displayed the destructive characters of crystalline material. Keiluweit et al. [56] reported that an increased in pyrolytic temperature from 100 °C to 300 °C reduced intensity of the peak of cellulose and it became broader as the cellulose decomposed gradually. Therefore, the sharp and narrow peaks of the XRD patterns Biochars A and B are crystalline with high degree of long-range peaks. The XRD diffraction patterns displayed distinct peaks of crystalline structure as the pyrolytic temperature increased (Fig. 3B and C).

3.6. Preliminary batch adsorption study and effect of pH

Elephant grass and Biochars A and B were used for uptake of nitrate ion from solution. Using 150 mg/L of nitrate solution of pH 2 and contact time of 8 h, the two biochars outperformed the elephant grass in the removal of nitrate. The data of this study are presented in Fig. S2. Elephant grass powder was able to adsorb 40 % of 150 mg/L of nitrate ion, however, Biochars A and B adsorbed approximately 91 % and 96 %, respectively. This observation is due to pyrolysis, which improved the features as well porosities of the Biochars A and B.

The initial pH of the adsorbate solution is a crucial influencing factor for determination of the interactions between adsorbate and adsorbent. For pH dependence experiments in this study, 150 mg/L of nitrate solution was used at 25 °C and contact time of 8 h. The dependence of percentage removal of nitrate on pH is presented in Fig. 4. It is evident that the variation of pH did not significantly influence percentage removal of nitrate ion by Biochars A and B. This observation is connected to the fact that adsorption mechanism was controlled by π–π interactions or van der Waals' interactions [63,64]. Since variation of pH on adsorption efficiency is insignificant, pH 7 was used for time and concentration dependence experiments. The two adsorbents can be used at any pH value, but pH of 7 is preferable because there is no fear of acidity or basicity since the pH of potable water is ≈ 7. This pH is also ideal for potable water treatment.

Table 3
Elemental mean composition of elephant grass and biochars.

	Elephant grass	Biochar A	Biochar B
C	30.11	54.29	57.55
N	9.49	3.54	3.79
O	41.85	19.31	17.89
Mg	0.21	0.68	0.51
P	0.54	0.71	0.56
S	0.50	0.76	0.88
K	15.00	10.20	8.65
Ca	–	1.32	0.95
Al	–	0.66	0.63
Si	3.12	6.06	5.96
Fe	–	0.90	–
Cl	1.19	1.20	1.79
Na	–	0.37	0.84
Cu	1.88	–	–

3.7. Kinetic analysis

One of the important influencing adsorption parameters is contact time. Rate constants, order of adsorption process and rate-determining steps are obtainable from the analysis of kinetic data. The kinetic dependence profiles for nitrate removal are shown in Fig. 5A and C, for Biochars A and B, respectively. The data in the profiles were obtained at pH 7 and 25 °C using 150 mg/L of nitrate solution. It is clear from the profiles that aqueous removal of nitrate ion is time dependent. This is supported by previous reports [26,30]. The adsorption was rapid initially until a plateau was reached after which adsorption of nitrate ion was independent of time. The amount of NO_3^- removed increased up to 40 min (Biochar A) and 50 min (Biochar B), this means that equilibrium was reached at an initial stage of the adsorption process.

Adsorption kinetics is a paramount factor for evaluation the dynamics of adsorption [65]. To investigate adsorption kinetic features of NO_3^- removal on Biochars A and B, the time-dependent data were subjected to kinetic models (pseudo-first order, pseudo-second order, Avrami fractional order, Elovich and intraparticle diffusion). Details of these models and the parameters (of data in Fig. 5) obtained from the models are presented in Table S2. The choice of the best model was done using the values of R^2_{adj}(adjusted determination coefficient) and SD (standard deviation). A high value (close to unity) of R^2_{adj}signifies good data fitting to a model. Hence, the higher the value of R^2_{adj}, the better the fit of the data to a choice model. In another view, the lower the SD value, the better the fitting. A low SD value means that both the theoretical (calculated) and the experimental values of the data are closer.

A careful study of the Table S2 reveals that the best model for the time-dependent data is Avrami fractional kinetic model, which is a 3-parameter empiric model that can be used to explain adsorption systems at solid-solution interface [66–69]. The model exhibited smallest difference between the calculated and experimental q values of all the models used in this study [64]. The values of the average fractional order (n_{AV}) for Biochars A and B are 0.5278 and 0.7192, respectively, while the values of Avrami kinetic constant (k_{AV}) are 0.2556 per min (Biochar A) and 0.08530 per min (Biochar B). The value of k_{AV} for Biochar A is higher than that of Biochar B by a factor of *ca.* 3. It is therefore expected that the rate of adsorption of Biochar A will be higher than that of Biochar B. The raw kinetic data, though not very visible in Fig. 5A and B, supported this assertion—Biochar A reached equilibrium earlier, by 10 min, than Biochar B. The equilibrium contact times of Biochars A and B are 40 min and 50 min, respectively. For equilibrium experiments on equilibrium study, contact of 60 min was used. The contact was increased to ensure that equilibrium will be reached at higher concentrations of nitrate ion [70,71].

To throw more light on kinetic of adsorption, the time-dependent

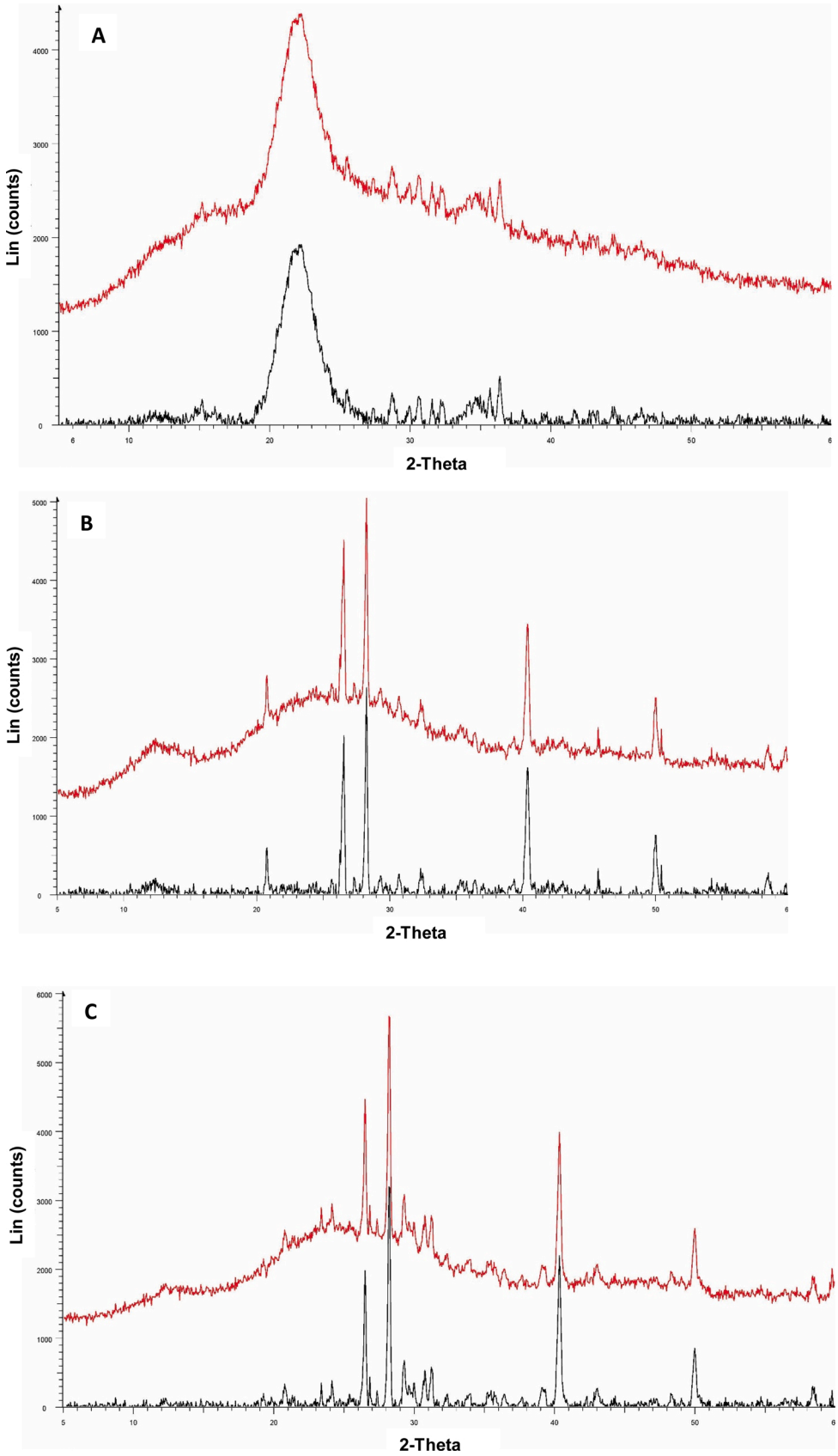

Fig. 3. X-ray diffraction patterns of elephant grass (A), Biochar A (B) and Biochar B (C).

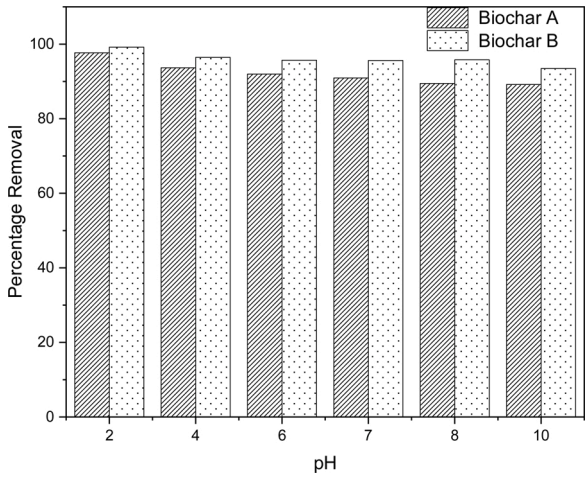

Fig. 4. Dependence of adsorption capacity of Biochar on pH for removal of nitrate ion.

data were subjected to intraparticle diffusion model (Table S2; Fig. 5B for Biochar A; Fig. 5D for Biochar B). The usage of this model enables one to explain effect of mass transfer resistance and identify the diffusion mechanism of binding of adsorbate onto adsorbent. As shown in Fig. 5B and D, the intraparticle diffusion curves had two linear segments for adsorption of nitrate ion onto the two biochars. The exhibition of two linear segments signifies that the adsorption process in this study had more than one adsorption rate. Thus, the first linear segment of the curves is attributed to the fast adsorption stage in which adsorbate molecules are transported to the surface of the adsorbent [72]. However, the other linear segment is regarded as the diffusion through small pores [72]. The second linear segment is attained after reaching equilibrium. The inability of the linear portions of the intraparticle diffusion plots to pass through the origin means that the diffusion mechanism was not the sole controlling mechanism of the adsorption process.

3.8. Equilibrium modelling

Typical concentration dependence profiles of adsorption of nitrate ion onto elephant grass biochars at 25 °C are presented in Fig. 6. The concentration dependence data were subjected to the Langmuir, Freundlich, Liu, and Redlich-Peterson equilibrium models. The respective equilibrium models are presented in Eqs (6–9).

$$q_e = \frac{q_{max} \cdot K_L \cdot C_e}{1 + K_L \cdot C_e} \tag{6}$$

$$q_e = K_F \cdot C_e^{1/n_F} \tag{7}$$

$$q_e = \frac{q_{max} \cdot (K_g \cdot C_e)^{nL}}{1 + (K_g \cdot C_e)^{nL}} \tag{8}$$

$$q_e = \frac{K_{RP} \cdot C_e}{1 + a_{RP} \cdot C_e^g} \text{ where } 0 < g \leq 1 \tag{9}$$

In the above models, K_L is the Langmuir equilibrium constant in L/mg, q_{max} is the maximum adsorption capacity of the biochar in mg/g, K_F is the Freundlich equilibrium constant in (mg/g (mg/L)$^{-1/nF}$), n_F is the

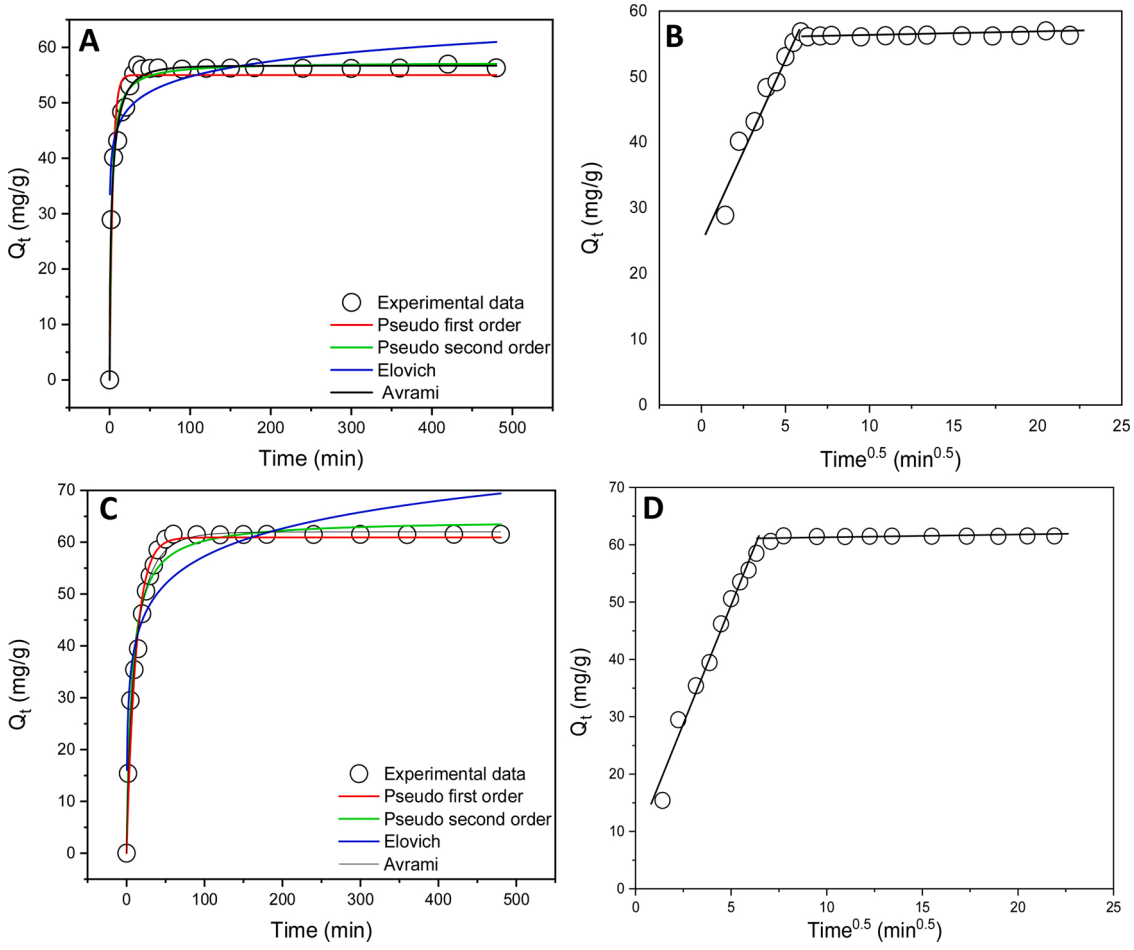

Fig. 5. Kinetic curves (A and C) and intraparticle diffusion plots (B and D) for adsorption of nitrate ion onto Biochar A (A and B) and Biochar B (C and D).

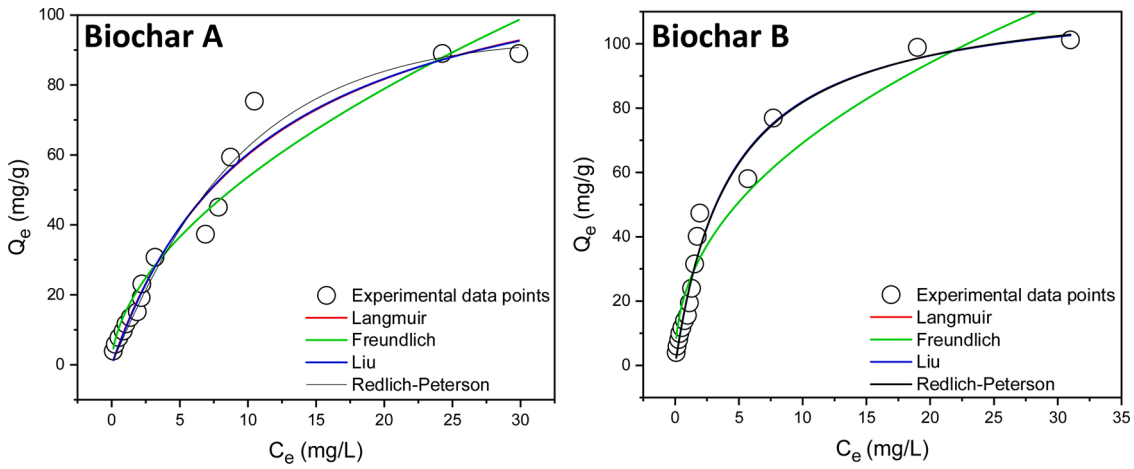

Fig. 6. Typical equilibrium curves for adsorption of nitrate ion onto Biochars A and B at 25 °C.

Freundlich dimensionless constant, K_g is the Liu equilibrium constant in L/mg, n_L is the Liu dimensionless exponent, K_{RP} is the Redlich–Peterson constant in L/g, a_{RP} is the Redlich–Peterson constant in $(mg/L)^{-g}$, and g is the Redlich–Peterson dimensionless exponent.

Equilibrium study provides relationship between concentration of adsorbate in solution and the amount of adsorbate adsorbed on the adsorbent surface when both liquid and solid phases are in equilibrium [73]. The modelling of equilibrium (concentration dependent) data into equilibrium models is important in adsorption studies because insights into relationship between adsorbate and adsorbent are obtained. Table S3 shows the various equilibrium parameters of the models used. The choice of the suitable model was done using the values of SD and R^2_{adj}. The Liu model is the best model that fitted the equilibrium data at all temperature ranges. Therefore, only the parameters of the Liu model will be discussed. The Liu adsorption equilibrium model, which is a 3-parameter model, combines the assumptions of Freundlich and Langmuir models. The values of q_{max} (maximum adsorption capacity) predicted by the Liu model are 140.7 mg g^{-1} at 35 °C for Biochar A and 237.5 mg g^{-1} for Biochar B at 50 °C. The value of K_g decreases as temperature increases, which denotes exothermic process. The n_L (Liu exponent) can have any positive value unlike g (Redlich-Peterson exponent) value, which must be in the range $0 < g \leq 1$. The values of n_L range between 0.9072 and 2.736 for Biochar A and between 0.6848 and 7.621 for Biochar B.

Table 4
Values of thermodynamic parameters of adsorption of nitrate ion onto elephant grass biochars.

Equation	Parameters	Units	Value for Biochar A	Value for Biochar B
$\Delta G^o = -RT\ln K_g$	R = gas constant = 8.314	J/mol K		
	T = absolute temperature	K		
	K = Liu equilibrium constant	–		
	ΔG° = standard Gibbs energy change at T = 298		–29.37	–27.01
	T = 303	kJ/mol	–28.69	–26.06
	T = 308		–28.96	–25.09
	T = 313		–28.20	–24.40
	T = 318		–26.76	–24.04
	T = 323		–25.88	–20.50
van't Hoff $\ln K_g = \frac{\Delta S^o}{R} - \frac{\Delta H^o}{R}\cdot\frac{1}{T}$	ΔH° = standard enthalpy change	kJ/mol	–69.97	–93.47
	ΔS° = standard entropy change	J/mol K	–135.252	–222.084
	R^2_{adj}	–	0.9410	0.9114

3.9. Thermodynamic analysis

The experiments on concentration dependence were repeated at different temperature values (25 °C – 50 °C). The data obtained were subjected to equilibrium modelling and the best model (Liu model) was identified. The Liu equilibrium constant, K_g, at various temperature values were converted into SI unit and used for evaluation of thermodynamic parameters together with temperature values in Kelvin. The thermodynamic parameters and van't Hoff plots are presented in Table 4 and Fig. S3, respectively. It is imperative to discuss influence of temperature on adsorption efficiency and calculate the thermodynamic parameters through which spontaneity, feasibility and other thermodynamic information of the adsorption process are obtained.

The values of ΔG° vary from –29.37 kJ/mol to –25.88 kJ/mol for Biochar A and from –27.01 kJ/mol to 20.50 kJ/mol for Biochar B. These values indicate that the adsorption of nitrate ion onto elephant grass biochars is spontaneous and feasible. The values of $\Delta H°$ are negative, which is an indication that adsorption process is exothermic. This is evident from the values of K_g shown in Table S3. The value of K_g decreases as temperature value increases—this observation is a feature of exothermic process. An increase in temperature lowers the values of equilibrium constant for exothermic processes. Going by the negative values of $\Delta S°$ in Table 4, it could be said that there was a reduction in disorderliness of the nitrate–biochar system. It can be concluded, from combined thermodynamic data, that adsorption of nitrate ion onto elephant grass biochars is a thermodynamically favourable process.

3.10. Comparison of adsorption capacities of various biochars for nitrate removal

The capacities of Biochars A and B to remove nitrate ion from aqueous solutions were compared with biochars produced from different types of biomass as shown in Table 5. Most of the biochars used for comparison were chemically modified to improve surface properties of the biochars and increase adsorption of nitrate from solution. It is important to reiterate that the biochars produced and used for nitrate removal in this study was not chemically modified because the biochars were also used for soil amendment (data not shown). The various data presented in Table 5 clearly indicate that the two elephant biochars have excellent adsorption efficiencies for nitrate ion uptake from solution. Biochars A and B have highest adsorption capacities than all other eights biochars (some of which were chemically modified) reported earlier for nitrate ion removal. Biochar B, which was pyrolysed at 600 °C,

Table 5
Data on nitrate removal using biochars reported in various studies.

Biochar type	Pyrolysis temperature (°C)	Maximum adsorption capacity (Q_m) in mg/g	Equilibrium model that predicted the Q_m	References
Corncobs (CC600)	600	14.46	Langmuir	[16]
Bamboo biochar/montmorillonite composite	460	8.516	Langmuir	[18]
Sawdust (SDB500)	500	1.574	Langmuir	[26]
Oak sawdust (CK-600)	600	8.940	Langmuir	[27]
Birch wood (NaClO oxidation and Acid wash)	700	3.970	Langmuir	[28]
Wheat straw (MgFe Layered double hydroxide)	600	24.80	Langmuir	[29]
Al-modified Soybean	500	40.63		[30]
Sugarcane bagasse	300	11.56	Langmuir	[40]
Elephant grass–B	600	237.5	Liu	*This study*

performed better than Biochar A (pyrolytic temperature of 400 °C) in the removal of nitrate ion from aqueous solutions. The usage of elephant biochars is recommended for efficient treatment of wastewater that contains high amounts of nitrate ion.

4. Conclusion

- An agricultural biomass, elephant grass, was successfully and gainfully converted to biochars using two pyrolytic temperatures of 400 °C (Biochar A) and 600 °C (Biochar B). Conversion of the biomass to biochars involved no chemical activation because the biochars were produced primarily for soil improvement.
- The two biochars possessed good carbon stability, water-holding capacity, cation exchange capacity, excellent porosity as well as abundant surface functional groups on the surface for nitrate binding and removal.
- Out of the pseudo-first order, pseudo-second order, Avrami fractional order and Elovich models used for analysis of the kinetic data, only Avrami model predicted the best kinetic parameters. Information from intraparticle diffusion analysis revealed that there were two adsorption stages which are: (1) migration of nitrate ion to the surface of the biochars, and (2) diffusion of nitrate molecules through small pores of biochars.
- The maximum adsorption capacities obtained from Liu equilibrium model are 140.7 and 237.5 mg g^{-1} for Biochars A and B, respectively.
- Adsorption of nitrate ion onto the biochars was spontaneous and exothermic. There was a reduction in randomness in the nitrate–biochar system.
- Elephant biochars are promising and low-cost alternative green adsorptive materials for aqueous nitrate removal.
- In general, high temperature of pyrolysis improved the characteristic features of biochars. Biochar pyrolysed at a high temperature performed better in the uptake of nitrate ion from water than the biochar pyrolysed at a lower temperature.
- Biochars can be produced in large quantities from elephant grass, which is widely available in most tropical regions. The two biochars prepared from elephant grass sufficiently removed nitrate ion from water. We intend to subject elephant grass biochars to various chemical activations/modifications for surface improvement in our next study.

5. Author statement

Florence M. Adesemuyi: conceptualization; investigation; methodology; data collection; and original draft of the manuscript. **Matthew A. Adebayo**: supervision; writing, data analysis and interpretation; editing; submission; and revision. **Adebisi O. Akinola**: formal analysis; development of methodology and supervision. **Emmanuel F. Olasehinde**: supervision and revision. **Kehinde A. Adewole**: development of methodology; and data curation. **Labunmi Lajide**: conceptualization; design of the work; supervision; and revision.

Declaration of Competing Interest

The authors report no declarations of interest.

Appendix A. Supplementary data

Supplementary material related to this article can be found, in the online version, at doi:https://doi.org/10.1016/j.jece.2020.104507.

References

[1] M.A. Adebayo, J.I. Adebomi, T.O. Abe, F.I. Areo, Removal of aqueous congo red and malachite green using Ackee apple seed–bentonite composite, Colloid Interface Sci. Commun. 38 (2020), 100311, https://doi.org/10.1016/j.colcom.2020.100311.

[2] A. Bazzo, M.A. Adebayo, S.L.P. Dias, E.C. Lima, J.C.P. Vaghetti, E.R. de Oliveira, A. J.B. Leite, F.A. Pavan, Avocado seed powder: characterization and its application as biosorbent for crystal violet dye removal from aqueous solutions, Desalin. Water Treat. 57 (2016) 15873–15888, https://doi.org/10.1080/19443994.2015.1074621.

[3] D. Wang, P. Jiang, H. Zhang, W. Yuan, Biochar production and applications in agro and forestry systems: a review, Sci. Total Environ. 723 (2020), 137775, https://doi.org/10.1016/j.scitotenv.2020.137775.

[4] IPCC (Intergovernmental Panel on Climate Change), IPCC Guidelines for National Greenhouse Gas Inventories, National Greenhouse Gas Inventories Programme, Hayama, Japan, 2006. www.ipcc-nggip.iges.or.jp/public/2006gl/index.html.

[5] A.K. Jain, J.R. Goss, Determination of reactor scaling factors for throatless rice husk gasifier, Biomass Bioenerg. 18 (2000) 249–256.

[6] C. Gai, Y. Dong, T. Zhang, Distribution of sulfur species in gaseous and condensed phase during downdraft gasification of corn straw, Energy 64 (2014) 248–258.

[7] P.N.D. Revilla, M.C. Maguyon-Detras, V.P. Migo, C.G. Alfafara, Nitrate removal from aqueous solution by adsorption using municipal solid waste-derived activated biochar, IOP Conf. Ser.: Mater. Sci. Eng. 778 (2020), 012135. https://1088/1757-899X/778/1/012135.

[8] Y.H. Hwang, D.G. Kim, H.S. Shin, Mechanism study of nitrate reduction by nano zero valent iron, J. Hazard. Mater. 185 (2011) 1513–1521.

[9] Q. Yin, H. Ren, R. Wang, Z. Zhao, Evaluation of nitrate and phosphate adsorption on Al-modified biochar: influence of Al content, Sci. Total Environ. 631–632 (2018) 895–903, https://doi.org/10.1016/j.scitotenv.2018.03.091.

[10] P. Li, K. Lin, Z. Fang, K. Wang, Enhanced nitrate removal by novel bimetallic Fe/Ni nanoparticles supported on biochar, J. Clean. Prod. 151 (2017) 21–33, https://doi.org/10.1016/j.jclepro.2017.03.042.

[11] World Health Organisation (WHO), Guidelines for Drinking Water Quality, 4th ed., 2011. Geneva.

[12] M. Kalaruban, P. Loganathan, W.G. Shima, J. Kandasamy, H.H. Ngo, S. Vigneswaran, Enhanced removal of nitrate from water using amine-grafted agricultural wastes, Sci. Total Environ. 565 (2016) 503–510, https://doi.org/10.1016/j.scitotenv.2016.04.194.

[13] R. Chintala, Javier Mollinedo, Thomas E. Schumacher, Sharon K. Papiernik, Douglas D. Malo, David E. Clay, Sandeep Kumar, Dylan W. Gulbrandson, Nitrate sorption and desorption in biochars from fast pyrolysis, Microporous Mesoporous Mater. 179 (2013) 250–257, https://doi.org/10.1016/j.micromeso.2013.05.023.

[14] C.T. Matos, A.M. Sequeira, S. Velizarov, J.G. Crespo, M.A.M. Reis, Nitrate removal in a closed marine system through the ion exchange membrane bioreactor, J. Hazard. Mater. 166 (2009) 428–434.

[15] S.E. Hale, V. Alling, J. Martinsen, Mulder, G.D. Breedveld, G. Cornelissen, The sorption and desorption of phosphate-P, ammonium-N and nitrate-N in cacao shell and corn cob biochars, Chemosphere 91 (2013) 1612–1619, https://doi.org/10.1016/j.chemosphere.2012.12.057.

[16] H. Zhao, Y. Xue, L. Long, X. Hu, Adsorption of nitrate onto biochar derived from agricultural residuals, Water Sci. Technol. 77 (2018) 548–554.

[17] F.A. Rutigliano, M. Romano, R. Marzaioli, I. Baglivo, S. Baronti, F. Miglietta, S. Castaldi, Effect of biochar addition on soil microbial community in a wheat crop, Eur. J. Soil Biol. 60 (2014) 9–15.

[18] E. Viglašová, M. Galamboš, Z. Danková, L. Krivosudský, C.L. Lengauer, R. Hood-Nowotny, G. Soja, A. Rompel, M. Matík, J. Briančin, Production, characterization and adsorption studies of bamboo-based biochar/montmorillonite composite for nitrate removal, Waste Manage. 79 (2018) 385–394, https://doi.org/10.1016/j.wasman.2018.08.005.

[19] Y.S. Sik, S.M. Uchimiya, M. Sophie, S.X. Chang, N. Bolan, Biochar: Production, Characterization and Applications, CRC Press, 2016. ISBN: 978-1-4822-4229-4.

[20] F. Sher, A. Yaqoob, F. Saeed, S. Zhang, Z. Jahan, K. JiříJaromí, Torrefied biomass fuels as a renewable alternative to coal in co-firing for power generation, Energy 209 (2020), 118444, https://doi.org/10.1016/j.energy.2020.118444.

[21] F. Sher, S.Z. Iqbal, S. Albazzaz, U. Ali, D.A. Mortari, T. Rashid, Development of biomass derived highly porous fast adsorbents for post-combustion CO_2 capture, Fuel 282 (2020), 118506, https://doi.org/10.1016/j.fuel.2020.118506.

[22] A.K.F. Vidal, T. Barbé, C. Da, R.F. Daher, J.E.A. Filho, R.S.N. de Lima, R.S. Freitas, D.A. Rossi, E.S. Oliveira, B.R. Menezes, G.C. Entringer, W.F.S. Peixoto, S. Cassaro, Production potential and chemical composition of elephant grass (*Pennisetum purpureum* Schum) at different ages for energy purposes, Afr. J. Biotechnol. 16 (2017) 1428–1433.

[23] R.F. Morais, D.M. Quesada, V.M. Reis, Contribution of biological nitrogen fixation to elephant grass (*Pennisetum purpureum* Schum), Plant Soil 349 (2011) 1–12.

[24] N.B. Dewage, A.S. Liyanagea, C.U. Pittman Jr., D. Mohan, T. Mlsna, Fast nitrate and fluoride adsorption and magnetic separation from water on α-Fe_2O_3 and Fe_3O_4 dispersed on Douglas fir biochar, Bioresour. Technol. 263 (2018) 258–265, https://doi.org/10.1016/j.biortech.2018.05.001.

[25] K. Kameyama, T. Miyamoto, Y. Iwata, T. Shiono, Influences of feedstock and pyrolysis temperature on the nitrate adsorption of biochar, Soil Sci. Plant Nutr. 62 (2016) 180–184, https://doi.org/10.1080/00380768.2015.1136553.

[26] L. Zhou, D. Xu, Y. Li, Q. Pan, J. Wang, L. Xue, A. Howard, Phosphorus and nitrogen adsorption capacities of biochars derived from feedstocks at different pyrolysis temperatures, Water 11 (2019) 1559, https://doi.org/10.3390/w11081559.

[27] Z. Wang, H. Guo, F. Shen, G. Yang, Y. Zhang, Y. Zeng, L. Wang, H. Xiao, S. Deng, Biochar produced from oak sawdust by Lanthanum (La)-involved pyrolysis for adsorption of ammonium (NH_4^+), nitrate (NO_3–), and phosphate (PO_4^{-3}), Chemosphere 119 (2015) 646–653, https://doi.org/10.1016/j.chemosphere.2014.07.084.

[28] J.R. Sanford, R.A. Larson, T. Runge, Nitrate sorption to biochar following chemical oxidation, Sci. Total Environ. 669 (2019) 938–947, https://doi.org/10.1016/j.scitotenv.2019.03.061.

[29] L. Xue, B. Ga, Y. Wan, J. Fang, S. Wang, Y. Li, R. Munoz-Carpena, L. Yang, High efficiency and selectivity of MgFe-LDH modified wheat-straw biochar in the removal of nitrate from aqueous solutions, J. Taiwan Inst. Chem. Eng. 63 (2016) 312–317, https://doi.org/10.1016/j.jtice.2016.03.021.

[30] Q. Yin, R. Wang, Z. Zhao, Application of Mg/Al-modified biochar for simultaneous removal of ammonium, nitrate, and phosphate from eutrophic water, J. Clean. Prod. 176 (2018) 230–240, https://doi.org/10.1016/j.jclepro.2017.12.117.

[31] A.S. Alsewaileh, A.R. Usman, M.I. Al-Wabel, Effects of pyrolysis temperature on nitrate-nitrogen (NO_3–N) and bromate (BrO_3–) adsorption onto date palm biochar, J. Environ. Manag. 237 (2019) 289–296, https://doi.org/10.1016/j.jenvman.2019.02.045.

[32] C.H. Chia, A. Downie, P. Munroe, Characteristics of biochar: physical and structural properties, in: J. Lehmann, S. Joseph (Eds.), Biochar for Environmental Management, 2nd ed., Routledge, New York, 2015, pp. 89–109.

[33] A. Usman, A. Sallam, M. Zhang, M. Vithanage, M. Ahmad, A. Al-Farraj, Y.S. Ok, A. Abduljabbar, M. Al-Wabel, Sorption process of date palm biochar for aqueous Cd (II) removal: efficiency and mechanisms, Water Air Soil Pollut. 227 (2016) 449, https://doi.org/10.1007/s11270-016-3161-z [Add to Citavi project by DOI].

[34] A.O. Akinola, Design of a Thermochemical Reactor for Conversion of Selected Wood Biomass to Fuel a Stationary Diesel Engine, A Ph.D Thesis at the Federal University of Technology, Akure, Nigeria, 2012.

[35] M.F. Adesemuyi, Pyrolysed Products From Lignocellulosic Wastes: Production, Characterisation and Their Effect on Soil Properties, Okra, Insect and Microbial Growth, a Ph.D Thesis, Department of Chemistry, The Federal University of Technology, Akure, Nigeria, 2020.

[36] M.C. Ribas, M. Franco, M.A. Adebayo, G.M. Parkes, E.C. Lima, L.A. Féris, Adsorption of Procion red MX-5B dye from aqueous solution using a homemade peach activated carbon compared with commercial activated carbon, Appl. Water Sci. 10 (6) (2020) 154, https://doi.org/10.1007/s13201-020-01237-9.

[37] C. Liu, W. Wang, Chemical looping gasification of pyrolyzed biomass and coal char with copper ferrite as an oxygen carrier, J. Renew. Sustain. Energy 10 (6) (2018), 063101.

[38] M. Yan, S. Zhang, H. Wibowo, N. Grisdanurak, Y. Cai, X. Zhou, E. Kanchanatip, Antoni, Biochar and pyrolytic gas properties from pyrolysis of simulated municipal solid waste (SMSW) under pyrolytic gas atmosphere, Waste Disposal Sustain. Energy 2 (2020) 37–46, https://doi.org/10.1007/s42768-019-00030-y.

[39] R.E. Masto, S. Kumar, T. Rout, P. Sarkar, J. George, L. Ram, Biochar from water hyacinth (*Eichornia crassipes*) and its impact on soil biological activity, Catena 111 (2013) 64–71.

[40] L.D. Hafshejani, A. Hooshmand, A.A. Naseri, S. Mohammadi, F. Abbasi, A. Bhatnagar, Removal of nitrate from aqueous solution by modified sugarcane bagasse biochar, Ecol. Eng. 95 (2016) 101–111, https://doi.org/10.1016/j.ecoleng.2016.06.035.

[41] C.H. Tsai, W.T. Tsai, S.C. Liu, Y.Q. Lin, Thermochemical characterization of biochar from cocoa pod husk prepared at low pyrolysis temperature, Biomass Convers. Biorefin. 8 (2018) 237–243.

[42] M.I. Al-Wabel, A. Al-Omran, A.H. El-Naggar, M. Nadeem, A.R. Usman, Pyrolysis temperature induced change in characteristic and chemical composition of biochar produced from *Cono carpus* wastes, Bioresour. Technol. 31 (2013) 374–379.

[43] J. Lehmann, J.P. da Silva Jr., C. Steiner, T. Nehls, W. Zech, B. Glaser, Nutrient availability and leaching in an archaeological Anthrosol and a Ferralsol of the Central Amazon basin: fertilizer, manure and charcoal amendments, Plant Soil 249 (2003) 343–357.

[44] H. Zhang, R. Voroney, G. Price, Effect of temperature and processing conditions on biochar chemical properties and their influence on soil C and N transformations, Soil Biol. Biochem. 83 (2015) 19–28.

[45] W. Song, M. Guo, Quality variations of poultry litter biochar generated at different pyrolysis temperature, J. Anal. Appl. Pyrol. 94 (2012) 138–145.

[46] T. Imam, S. Capareda, Characterization of bio-oil, syn-gas and bio-char from switchgrass pyrolysis at various temperatures, J. Anal. Appl. Pyrol. 93 (2012) 170–177.

[47] I.U. Hai, F. Sher, A. Yaqoob, H. Liu, Assessment of biomass energy potential for SRC willow woodchips in a pilot scale bubbling fluidized bed gasifier, Fuel 258 (2019), 116143, https://doi.org/10.1016/j.fuel.2019.116143.

[48] F. Sher, S.Z. Iqbal, H. Liu, M. Imran, C.E. Snape, Thermal and kinetic analysis of diverse biomass fuels under different reaction environment: a way forward to renewable energy sources, Energy Convers. Manage. 203 (2020), 112266, https://doi.org/10.1016/j.enconman.2019.112266.

[49] M. Ahmad, S.S. Lee, X. Dov, D. Mohan, J.K. Sung, J.E. Yang, Y.S. Ok, Effects of pyrolysis temperature on soy bean storer and peanut shell- derived biochar properties and TCE adsorption in water, Bioresour. Technol. 118 (2012) 536–544.

[50] M. Uchimiya, L.H. Wartelle, K.T. Klasson, C.A. Fortier, I.M. Lima, Influence of pyrolysis temperature on biochar property and function as a heavy metal sorbent in soil, J. Agric. Food Chem. 59 (2011) 2501–2510.

[51] J.M. Novak, I. Lima, B. Xing, J.W. Gaskin, C. Steiner, K.C. Das, M. Ahmedna, D. Rehrah, D.W. Watts, W.J. Busscher, H. Schomberg, Characterization of designer biochar produced at different temperatures and their effects on a loamy sand, Ann. Environ. Sci. 3 (2009) 195–206.

[52] N. Claoston, A.W. Samsuri, M.H. Ahmad-Husni, M.S. Mohd-Amran, Effects of pyrolysis temperature on the physicochemical properties of empty fruit bunch and rice husk biochar, Waste Manage. Resour. 32 (2014) 331–339.

[53] K.B. Cantrell, P.G. Hunt, M. Uchimiya, Impact of pyrolysis temperature and manure source on physicochemical characteristics of biochar, Bioresour. Technol. Rep. 107 (2012) 419–428.

[54] Y. Yao, B. Guo, M. Inyang, Biochar derived from anaerobically digested sugar organofunctionalized layered silicate for textile dye removal, J. Hazard. Mater. 181 (2011) 366–374.

[55] L. Yang, M. Jin, C. Tong, S. Xie, Study of dynamic sorption and desorption of polycyclic aromatic hydrocarbons in silty-clay soil, J. Hazard. Mater. 244–245 (2013) 77–85.

[56] M. Keiluweit, P.S. Nico, M.G. Johnson, M. Kleber, Dynamic molecular structure of plant-derived black carbon (Biochar), Environ. Sci. Technol. 44 (2010) 1247–1253.

[57] K. Sun, K. Ro, M.X. Guo, J. Novak, H. Mashayekhi, B. Xing, Sorption of bisphenol A, 17a–ethinyl estradiol and phenanthrene on thermally and hydrothermally produced biochars, Bioresour. Technol. 102 (2011) 5757–5763.

[58] B. Chen, D. Zhou, L. Zhu, Transitional adsorption and partition of nonpolar and polar aromatic contaminants by biochars of pine needles with different pyrolytic temperatures, Environ. Sci. Technol. 42 (2008) 5137–5143.

[59] X. Cao, W. Harris, Properties of dairy-manure-derived biochar pertinent to its potential use in remediation, Bioresour. Technol. 101 (2010) 5222–5228.

[60] A. Shaaban, Se. Sian-Meng, M. Nona, M. Mitan, M.F. Dimin, Characterization of biochar derived from rubber wood sawdust through slow pyrolysis on surface porosities and functional groups, Procedia Eng. 68 (2013) 365–371.

[61] A. Downie, A. Crosky, P. Munroe, Physical Properties of Biochar, Biochar for Environment Management, Science and Technology, Earthscan, London UK, 2009.

[62] R. Qadeer, J. Hanif, M.A. Saleem, M. Afzal, Characterization of activated charcoal, J. Chem. Soc. Pakistan 16 (1994) 229–235.

[63] L.A. Rodrigues, M.L.C.P. da Silva, M.O. Alvarez-Mendes, A.R. Coutinho, G.P. Thim, Phenol removal from aqueous solution by activated carbon produced from avocado kernel seeds, Chem. Eng. J. 174 (2011) 49–57.

[64] P.S. Thue, M.A. Adebayo, E.C. Lima, J.M. Sieliechi, F.M. Machado, G.L. Dotto, J.C. P. Vaghetti, S.L.P. Dias, Preparation, characterization and application of microwave-assisted activated carbons from wood chips for removal of phenol from aqueous solution, J. Mol. Liq. 223 (2016) 1067–1080, https://doi.org/10.1016/j.molliq.2016.09.032.

[65] A. Kausar, F. Sher, A. Hazafa, A. Javed, M. Sillanpää, M. Iqbal, Biocomposite of sodium-alginate with acidified clay for wastewater treatment: kinetic, equilibrium and thermodynamic studies, Int. J. Biol. Macromol. 161 (2020) 1272–1285, https://doi.org/10.1016/j.ijbiomac.2020.05.266.

[66] Z. Knezevic, L. Mojovic, B. Adnadjevic, Palm oil hydrolysis by lipase from *Candida cyhdracea* mmobilized on zeolite type Y, Enzyme Microb. Technol. 22 (1998) 275–280.

[67] E.C. Lima, M.A. Adebayo, F.M. Machado, Kinetic and equilibrium models of adsorption, in: C.P. Bergmann, F.M. Machado (Eds.), Carbon Nanomaterials as Adsorbents for Environmental and Biological Applications, Springer International Publishing, New York, 2015, pp. 33–69, https://doi.org/10.1007/978-3-319-18875-1_3.

[68] E.C. Lima, A.R. Cestari, M.A. Adebayo, Comments on the paper: a critical review of the applicability of Avrami fractional kinetic equation in adsorption-based water treatment studies, Desalin. Water Treat. 57 (2016) 19566–19571, https://doi.org/10.1080/19443994.2015.

[69] E.C.N. Lopes, F.S.C. dos Anjos, E.F.S. Vieira, A.R. Cestari, An alternative Avrami equation to evaluate kinetic parameters of the interaction of Hg(II) with thin chitosan membranes, J. Colloid Interface Sci. 263 (2003) 542–547.
[70] S. Rovani, A.N. Fernandes, L.D.T. Prola, E.C. Lima, W.O. Santos, M.A. Adebayo, Removal of Cibacron Brilliant Yellow 3G-P Dye from aqueous solutions by Brazilian peats as biosorbents, Chem. Eng. Comm. 201 (2014) 1431–1458, https://doi.org/10.1080/00986445.2013.816954.
[71] M.A. Adebayo, Adsorption of congo red from aqueous solutions using clay–corn cob–$FeCl_3$ composite, FUTA J. Res. Sci. 15 (1) (2019) 61–74.
[72] M.A. Adebayo, L.D.T. Prola, E.C. Lima, M.J. Puchana-Rosero, R. Cataluña, C. Saucier, C.S. Umpierres, J.C.P. Vaghetti, L.G. Da Silva, R. Ruggiero, Adsorption of Procion Blue MX-R dye from aqueous solutions by lignin chemically modified with aluminium and manganese, J. Hazard. Mater. 268 (2014) 43–50, https://doi.org/10.1016/j.jhazmat.2014.01.005.
[73] G.S. dos Reis, M.A. Adebayo, E.C. Lima, C.H. Sampaio, L.D.T. Prola, Activated carbons from sewage sludge for preconcentration of copper, Anal. Lett. 49 (2016) 541–555, https://doi.org/10.1080/00032719.2015.1076833.